Stability studies of starch aerogel formulations for biomedical applications

*Víctor Santos-Rosales[1], Gerardo Alvarez-Rivera[2], Markus Hillgärtner[3], Alejandro Cifuentes[2], Mikhail Itskov[3], Carlos A. García-González[1,] * and Ameya Rege[4,]* **

[1] Department of Pharmacology, Pharmacy and Pharmaceutical Technology, I+D Farma group (GI-1645), Faculty of Pharmacy, Health Research Institute of Santiago de Compostela (IDIS), Agrupación Estratégica de Materiales (AeMAT), Universidade de Santiago de Compostela, E-15782 Santiago de Compostela, Spain.

[2] Laboratory of Foodomics, Institute of Food Science Research, CIAL, CSIC, Nicolás Cabrera 9, 28049 Madrid, Spain.

[3] Department of Continuum Mechanics, RWTH Aachen University, Eilfschornsteinstr. 18, 52062 Aachen, Germany

[4] Department of Aerogels and Aerogel Composites, Institute of Materials Research, German Aerospace Center (DLR), Linder Höhe, 51147 Cologne, Germany

ABSTRACT: Starch aerogels are attractive materials for biomedical applications due to their low density and high open porosity coupled with high surface areas. However, the lack of macropores in conventionally-manufactured polysaccharide aerogels is a limitation to their use as scaffolds for regenerative medicine. Moreover, the stability under storage of polysaccharide aerogels is critical for biomedical purposes and scarcely studied so far. In this work, the induction of a new macropore population (1-2 μm) well-integrated in the starch aerogel backbone was successfully achieved by the incorporation of zein as a porogen. The obtained dual-porous aerogels were evaluated in terms of composition as well as morphological, textural and mechanical properties. Stability of aerogels upon storage mimicking the zone II (25 ºC, 65 % relative humidity) according to International Conference on Harmonization (ICH) guideline of climatic conditions was checked after 1 and 3 months from morphological, physicochemical and mechanical perspectives. Zein incorporation induced remarkable changes in the mechanical performance of the end aerogel products and showed a preventive effect on the morphological changes during the storage period.

INTRODUCTION

The development of innovative synthetic grafts, known as scaffolds, offers a promising response to regenerate damaged tissues encouraging the self-healing capacity of the patients. Depending on the anatomical target, scaffolds must display a particular 3D interconnected and hierarchical porous structure for an appropriate performance once implanted [1–3]. Moreover, the mechanical behavior of the grafts is of particular relevance since they should temporarily surrogate the requirements of the natural tissue.

Aerogels are solid mesoporous materials characterized by extremely low densities and high open porosities of tailored size and distribution [5,6]. These properties of aerogels have been widely exploited in several fields, particularly silica and carbon aerogels in the building industries as thermal insulation materials [7–9]. Nevertheless, bio-based aerogels (i.e. from polysaccharides and proteins) are the mainstream choice for biomedical applications. In particular, starch aerogels emerge as an attractive alternative for bone scaffolds, where the advanced properties of aerogels are supplemented by the biocompatibility, the complete physiological degradation and the abundance of starch in nature [10–12]. In addition, starch-based blends promote cell adhesion and proliferation using human osteoblasts [13,14].

Starch aerogels are formed by a network of intermingled fibers of amylose and amylopectin with a defined micro/mesoporous architecture that can mimic the extracellular matrix. Nevertheless, the usual absence of pores in the macroscale (1 μm and above) hampers the interaction of the scaffold with the biological tissue. The addition of sacrificial porogens (e.g., salts, sugar or paraffin wax) of defined shapes and dimensions has been explored to confer macroporosity to different aerogel sources [15–18]. However, these approaches result in tedious and

cumbersome protocols for aerogel processing requiring additional leaching steps to remove the porogen.

Stability studies are mandatory for conventional drug products and medical devices to verify that raw materials and end products meet the legal requirements in terms of identity, output, quality and purity over time [19]. Stability in terms of chemical identity, physical form and biological activity, is a critical parameter that could prevent the clinical use and that gives practical information to decide on the need and choice of primary and secondary packaging for the product. However, there is a paucity of information focused on the effect of the storage period on the performance of nanostructured scaffolds, although those with intricate geometries are particularly affected by environmental conditions.

In this work, starch-based aerogels endowed with macroporosity were obtained through an innovative processing approach involving the use of porogens without extra-leaching steps. Zein, the major protein of storage of corn, was tested as porogen to induce the formation of well-integrated macropores in the mesoporous starch aerogel network. The effect of the use of zein was evaluated on the resulting aerogel composition, textural and mechanical properties. In addition, quantitative determinations of zein residues in the aerogels were performed, since its presence favor the *in vivo* promotion of mesenchymal stem cells adhesion and proliferation [20,21]. The stability upon storage was studied on a mid-term (1 and 3 months) mimicking the zone II International Conference on Harmonization (ICH) guideline of climatic conditions (25 ºC, 60 % relative humidity) [22], which corresponds to the worst case storage scenario for the regions of Europe, Japan and USA. Scaffolds were monitored in terms of morphological, physicochemical and mechanical stability.

MATERIALS AND METHODS

Materials. Native corn starch (52.6 % amylose content, ρ_{skel}= 1.4562 ± 0.012 g/mL) was provided by Roquette Frères S.A. (Lestrem, France). Zein (m.p. 266-283 °C, size of dry agglomerates by the sieving method: 557 ± 208 µm; ρ_{skel}= 1.167 ± 0.025 g/mL) was purchased from Sigma-Aldrich, Inc. (Madrid, Spain). CO_2 (purity > 99.9 %) was supplied by Praxair, Inc. (Madrid, Spain). Absolute ethanol (EtOH) was provided by VWR (Radnor, PA, USA).

Corn starch aerogels preparation. Cylindrical aerogel specimens were obtained by adapting a previously reported procedure [23]. Briefly, starch-aqueous dispersions (10 % w/w) containing varying ratios of zein as porogen (Table 1) were subjected to a thermal treatment for starch gelatinization (121 °C, 20 min) and dosed in cylindrical polypropylene molds (length: 14 mm, diameter: 12 mm). After storage at 4 °C for 48 h, the resulting gels were immersed in absolute ethanol for solvent exchange (gel-alcogel transition) and zein leaching. Solvent was replaced with fresh ethanol six times at an exchange frequency of 48 h. Starch alcogels were then loaded in a 100 mL autoclave (Thar Process, Pittsburg, PA, USA) containing 45 mL of absolute ethanol. A continuous flow of 6 g/min of supercritical CO_2 (40 ºC, 130 bar) through the autoclave during 4 h was employed for ethanol extraction. Subsequently, a controlled depressurization of 2 bar/min until atmospheric pressure was performed. Aerogel cylindrical probes (length: *ca.* 11 mm, diameter: *ca.* 8.5 mm) were collected from the autoclave for further characterization.

Table 1. Starch aerogel notation regarding the initial content of starch and zein (expressed in grams and in weight ratios) used in the batches for the hydrogel formation.

Aerogel	Zein-to-starch weight ratio	c (*see Eq. 4*)
Z0	0 g : 8 g (0:1)	0
Z1	2 g : 8 g (1:4)	0.25

Z2	4 g : 8 g (1:2)	0.5
Z3	6 g : 8 g (3:4)	0.75
Z4	8 g : 8 g (1:1)	1

Analytical, physicochemical, structural and mechanical characterization of starch aerogels. The volume reduction (ΔV, in percentage) of the gels after the solvent exchange and the supercritical drying steps was evaluated as

$$\Delta V = \left(\frac{V_0 - V}{V_0}\right) \text{ x } 100 \quad (1)$$

where Vo denotes the initial volume of the hydrogel and V the end volume of the alcogel or aerogel, accordingly.

For zein residues quantification in the aerogels, a bottom-up proteomics approach was applied, involving proteolytic digestion of zein before high-resolution tandem-mass spectrometry analysis. Starch aerogel samples were dissolved at a concentration of 1 mg/mL in buffer solution A (10 mM Tris–HCl pH 8.0, 8 M urea) under agitation overnight. Dissolved samples were diluted in buffer solution B (50 mM Tris–HCl pH 8.0, 0.5 mM $CaCl_2$) in order to reach urea concentrations below 6 M. For zein proteins digestion, 370 µL of the previous sample solution were mixed with 120 µL of thermolysin stock solution prepared in buffer solution B (enzyme-to-substrate weight ratio 1:20), and incubated for 1 h at 80 ºC in an Eppendorf ThermoMixer (Eppendorf AG, Hamburg, Germany). The digestion reaction was stopped by adding 25 µL of formic acid (10 vol.%). Digested solutions were filtered through a Microcon-30 kDa Centrifugal Filter (Merck KGaA, Darmstadt, Germany) before analysis to remove non-digested proteins.

An Agilent 1290 UHPLC system coupled to an Agilent 6540 quadrupole-time-of-flight mass spectrometer (q-TOF MS) and equipped with an orthogonal ESI source was employed for the determination and quantification of zein residues. Chromatographic separation of digested zein

was conducted using a Zorbax Eclipse Plus C18 column (2.1 × 100 mm, 1.8 µm particle diameter, Agilent Technologies, Santa Clara, CA, USA) at 30 °C. The mobile phase was composed of water (0.1 vol.% formic acid, solvent A) and acetonitrile (0.1 vol.% formic acid, solvent B). A 5-µL aliquot of the sample was injected at a flow rate of 0.5 mL/min during gradient elution. The gradient program was as follows: 0 min, 0 % B; 7 min, 30 % B; 9 min, 80 % B; 11 min, 100 % B; 13 min, 100 % B; 14 min, 0 % B. The mass spectrometer was operated in MS and MS/MS modes. MS parameters were the following: capillary voltage, 4000 V; nebulizer pressure, 40 psi; drying gas flow rate, 10 L/min; gas temperature, 350 ºC; skimmer voltage, 45 V; fragmentor voltage, 110 V. The MS and Auto MS/MS modes were set to acquire m/z values ranging between 50-1100 and 50-800, respectively, at a scan rate of 5 spectra per second. Operating the ESI source in positive ionization mode, four proteolytic peptides were monitored: LQQQ (m/z 516.2776), LQQ (m/z 388.2190), FNQ (m/z 408.1877) and FSQ (m/z 381.1768).

Skeletal density of starch aerogels (ρ_{skel}) was determined by helium pycnometry (Quantachrome, Boynton Beach, FL, USA) at room temperature (25 °C) and 1.01 bar. Values were obtained from five replicates (standard deviation < 4 %). Bulk density of the aerogels (ρ_{bulk}) was determined by weighing and measuring their dimensions. The resulting overall porosity (ε) and total pore volume were calculated from Eqs. (2) and (3), respectively.

$$\varepsilon = \left(1 - \frac{\rho_{bulk}}{\rho_{skel}}\right) \text{x } 100 \quad (2)$$

$$V_p = \left(\frac{1}{\rho_{bulk}} - \frac{1}{\rho_{skel}}\right) \quad (3)$$

Textural properties of the aerogels were determined by N_2 adsorption-desorption analyses (ASAP 2000 Micromeritics Inc, Norcross, GA, USA). Prior to the measurements, aerogels were outgassed at 80 °C and under vacuum (<1 mPa) for 24 h. Specific surface area (A_{BET}) of the aerogels scaffolds were determined by the Brunauer-Emmett-Teller (BET) method. Specific pore

142 volumes ($V_{p,BJH}$) and mean pore diameter ($d_{p,BJH}$) were evaluated from the desorption branch of
143 the isotherms using the Barrett-Joyner-Halenda (BJH) method (Figure S1).
144 Based on the BJH-pore volume distribution, the contributions (in percentage) of mesopores (2-
145 50 nm range, $V_{p,meso}$) to the total pore volume were determined. The contribution of the
146 macropore population (>50 nm, $V_{p,macro}$) was determined by the difference between the total
147 specific pore volume and the specific mesopore volume (Vp,meso).
148 The structure of the aerogels was evaluated by scanning electron microscopy (FESEM,
149 ULTRA-PLUS, Zeiss, Oberkochen, Germany) running at 3 kV. Prior to imaging, aerogels were
150 sputtered with a layer of iridium of 10 nm thickness.
151 The mechanical behavior of cylindrical aerogel specimens was analyzed by means of uniaxial
152 quasistatic compression tests using a 10 kN load cell on the universal testing machine Z010
153 (Zwick/Roell GmbH, Ulm, Germany). The strain rate of 10 %/min was applied for all
154 compression tests. To characterize the inelastic features of the aerogels, cyclic compression was
155 conducted, whereby the aerogel specimens were subjected to three sets of loading and unloading
156 cycles with the strain amplitude increased stepwise by 20 %. All the experiments were
157 performed at 20 °C, atmospheric pressure and in triplicate.
158
159 **Stability tests under storage of starch aerogels.** Aerogel cylindrical probes of each
160 composition were placed inside sterile glass vessels with hermetic closure, containing a solution
161 of sulfuric acid (37 % v/v) to maintain the relative humidity at 65 % [24]. Containers were stored
162 for either 1 or 3 months at 25 °C. After the storage time was elapsed, aerogels were collected for
163 their complete characterization.

Statistical analysis. All results were expressed as mean ± standard deviation. Statistical analyses of shrinkage values (1-way ANOVA) were performed followed by the post hoc Tukey-Kramer method test using Statistica v.8.0 software (StatSoft Inc., Tulsa, OK, USA)

RESULTS AND DISCUSSION

Morphological and physicochemical characterization of starch-based macroporous aerogels. Corn starch aerogels were prepared in the form of cylindrical monoliths for a reproducible determination of their densities and mechanical properties. White solid lightweight structures were obtained in all cases, although the modified starch aerogels showed a slight yellow coloration suggesting the presence of zein residues (Figure S2). The use of zein favored the homogeneous dosing of the aqueous dispersion in the moulds. The reduced content of amylose in the admixture extended its retrogradation rate since less intermolecular hydrogen-bondings were formed within the dispersion [11,25].

A determination method based on a bottom-up approach was set up to quantify zein residues in the aerogel samples. The full sequence of 19 kDa alpha-zein 19C2 (ZEA9 MAIZE – P06677) protein was obtained from Uniport database, and the whole sequence of peptides was exported to PeptideMass tool from ExPasy website for *in silico* digestion. Theoretical peptide masses of the input proteins were generated applying the following stringent criteria: thermolysin was selected as digestion enzyme, and only one missed cleavage was allowed for thermolysin digestion.

Operating the HPLC-ESI-QTOF system in the positive ionization mode (ESI+), a targeted screening analysis in full MS mode (m/z 100–1100 mass range) was performed to identify the m/z $[M+H]^+$ peptide masses obtained from *in silico* digestion in a zein standard solution and in the starch aerogel sample theoretically containing the highest zein content (Z4). Figure 1 shows

four selected zein peptides masses (m/z = 516.2776 $[LQQQ+H]^+$ 388.2190 $[LQQ+H]^+$; 408.1877 $[FNQ+H]^+$; 381.1768 $[FSQ+H]^+$) in Z4 sample. Theses peptides were selected for zein determination, exhibiting satisfactory intensity, sensitivity and dynamic range.

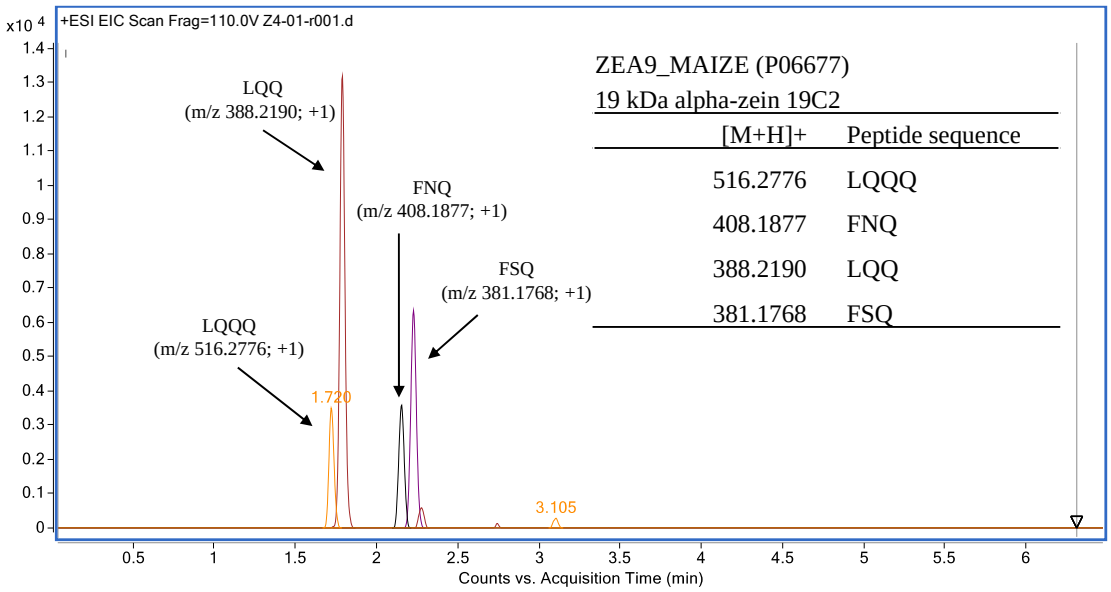

Figure 1. High-resolution extracted ion chromatograms (HREICs) of Z4 starch aerogel, showing the target peptides masses (10 ppm extraction window) for zein residues determination in aerogels.

Table 2 shows the main LC-HRMS parameters for the target peptides, including chromatographic retention time, monoisotopic mass, protonated molecular ion and calculated mass error (Δm/z). The identification of zein peptides was based on identity of the exact mass, monoisotopic profile and MS/MS fragmentation spectra (Figure S3). Zein content in Z0-Z4 starch aerogels was determined by external standard calibration using a zein standard solution submitted to the same digestion process as the starch samples (see Table 2).

Table 2. HPLC-HRMS parameters of target zein peptide fragment. Concentration values (% w/w) for zein residues in different starch aerogels.

RT (min)	Peptide sequence	Formula	Monoisotopic mass	[M+H]+ (m/z)	Error (ppm)	Concentration in starch (%, w/w ± std)				
						Z0	Z1	Z2	Z3	Z4
1.719	LQQQ	C21H37N7O8	515.2704	516.2776	1.0	nd	4.0±0.1	13.5±0.1	12.8±1.1	27.4±0.9
1.795	LQQ	C16H29N5O6	387.2118	388.2190	3.6	nd	3.3±0.1	9.9±0.2	10.4±0.3	21.2±0.2
2.153	FNQ	C18H25N5O6	407.1805	408.1877	1.5	nd	3.8±0.1	11.3±0.7	12.3±1.0	25.5±0.2
2.229	FSQ	C17H24N4O6	380.1696	381.1768	4.2	nd	3.7±0.4	7.2 ±0.5	11.1±1.1	21.1±0.9
Average zein concentration						nd	3.7±0.3	10.5± 2.6	11.6±1.1	23.8±3.1

All the manufactured starch aerogels had a certain volume shrinkage mainly during the solvent exchange step and, in a lesser extent, during the supercritical drying step (Figure 2). The addition of the zein in the aerogels strongly reduced the shrinkage values, particularly during gel-alcogel transition. For instance, a 4-fold reduction in these values was observed for Z4 aerogels. However, this effect was not linear and aerogels with similar residual zein content (Z2, Z3, in Table 2) behaved differently. On the other hand, the volume reduction detected during the supercritical drying was severe, although the overall shrinkage values are in accordance with those reported for starch aerogels with similar amylose contents (30-40 %) [26,27]. Interestingly, Z1 aerogels presented similar values to Z4, despite of the fact that zein residues were much higher in the latter formulation.

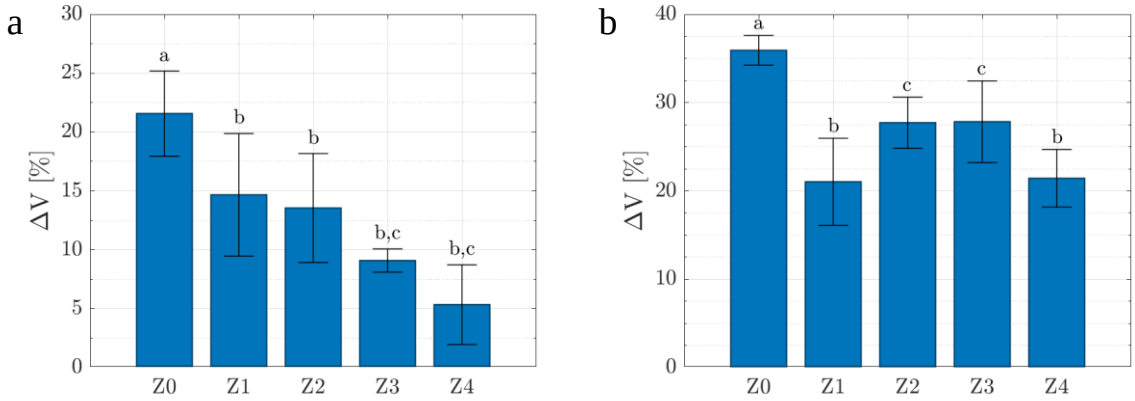

Figure 2. Volume shrinkage of starch-based gels after (a) the solvent exchange and (b) supercritical drying. Equal letters denote statistically homogeneous groups.

Bulk densities of the obtained aerogels (ρ_{bulk}) strongly depended on the initial hydrogel composition (Table 3). Aerogel formulations prepared from hydrogels with lower zein contents (Z1, Z2) were significantly lighter (*ca*. 30%) than pure starch aerogels (Z0) ($p>0.05$). Conversely, denser structures were proportionally obtained with zein content when the 1:2 zein-to-starch weight ratio was exceeded for the Z2-Z3-Z4 aerogel sequence. The remaining zein residues are responsible for this effect as depicted in Table 2. For example, Z3 presented almost identical density values to the unmodified formulations (Z0), whereas Z4 aerogels were the heaviest structures. Accordingly, the overall porosity of the aerogels (ε) followed a reverse trend with respect to the bulk density, but falling in the 85-91 % range in all cases, which is advantageous for regenerative medicine applications as scaffold matrices [28].

The technical feasibility of the processing strategy to induce a larger pore population in starch aerogels was confirmed from the textural analysis (Table 3). The zein addition in the aerogel formulations resulted in increased specific surface areas (A_{BET} = 183-228 m^2/g) with values in the range of those reported for high amylose corn starch aerogels [12,26,29]. Similarly, the specific pore volume ($V_{p,BJH}$) was higher as the porogen content increased while the mean pore diameter

($d_{p,BJH}$) remained constant at 18-20 nm. The formation of dual porous aerogels was confirmed from the macropore contribution to the overall porous values ($V_{p,macro}$ in Table 3). The total pore volume and macropore contribution were determined by the combination of N_2 adsorption-desorption and helium pycnometry analyses, since the contribution of macropores in the pore volume (over 80 % of the overall porosity for other bio-aerogels [30,31]), may not be taken into account in the characterization of aerogels through the BJH method. The zein effect in macropore formation is clearly appreciated from Z0 to Z2 aerogels by an increase in $V_{p,macro}$ of up to 4 %. Conversely, $V_{p,macro}$ values for Z3 and Z4 aerogels were similar and 10 % lower than that ones for unmodified aerogels (Z0). Although most of the porogen was leached during the solvent exchange step, the zein residue of 10 to 20 wt.% quantified in the abovementioned formulations is responsible for their densification and thus directly decreasing the pore volume V_p since it is a specific parameter (i.e. expressed in a mass basis). (Table 3).

Scanning electron microscopy (SEM) images of starch aerogels confirmed that their morphology and texture were dramatically influenced by the presence of zein porogen in the aerogel processing (Figure 3). The unmodified aerogel (Z0) presented an interconnected fiber network in the 30-60 nm diameter range (Figures 3a,b) typical for starch aerogels [32]. The incorporation of zein during the aerogel processing induced remarkable morphological changes to the aerogel architectures with the presence of spherical macropores (*ca.* 2 μm) even in the formulation with lower zein content (Z1 in Figures 3c,d). This new pore family presented inner rough surfaces, but the presence of a thin film in certain pores (Figure 3d) suggested an incomplete zein removal during the solvent exchange step. The observed morphology was thus coherent with the zein quantifications (Table 2). The thermal treatment for the starch gelatinization disrupts the close-packed tertiary globular structure of zein, increasing its water

254 soluble fraction and promoting the formation of disulphide bonds [33–35]. Therefore, the formation
255 of zein agglomerates are favored due to the higher interactions between polypeptide chains [36,37].
256 Z2 aerogels presented regions of large protein aggregates (>10 μm) and also regions of perfectly
257 integrated dual and interconnected porosity (Figures 3e,f). Aerogels prepared with higher
258 contents of porogen led to more irregular structures (Z3 in Figures 3g,h, and Z4 in Figures 3i,j),
259 supporting the increased specific surface areas values (A_{BET} in Table 3). The formation of larger
260 pores in Z3 aerogels was clearly identified as the footprint of zein particles after the leaching
261 (Figure 3g). The remaining globular zein residues embedded in the starch mesoporous backbone
262 were also observed (Figure 3h). The presence of porous zein films was more abundant in Z4
263 formulation (Figure 3i). Overall, the formation of a family of large (1-3 μm) and interconnected
264 macropores was achieved through the use of zein as porogen (Figure 3j).
265
266

Table 3. Morphological and textural properties of the obtained aerogels. Values expressed as mean values and standard deviation.

Aerogel		ρ_{bulk} (g/mL)	ρ_{skel} (g/mL)	ε (%)	A_{BET} (m^2/g)	$V_{p,BJH}$ (cm^3/g)	$d_{p,BJH}$ (nm)	V_p (cm^3/g)	$V_{p,meso}$ (%)	$V_{p,macro}$ (%)
Z0	*No storage*	0.175 ± 0.004	1.478 ± 0.05	88.1 ± 0.4	183 ± 9	1.01 ± 0.05	19.1 ± 1.0	5.03	15.1	84.9
	1 month	0.200 ± 0.005	1.495 ± 0.03	86.6 ± 0.4	217 ± 11	1.30 ± 0.07	21.6 ± 1.1	4.33	20.8	79.2
	3 months	0.184 ± 0.006	1.467 ± 0.03	87.5 ± 0.4	213 ± 11	1.30 ± 0.06	23.3 ± 1.2	4.76	18.6	81.4
Z1	*No storage*	0.120 ± 0.013	1.349 ± 0.02	91.1 ± 1.0	228 ± 11	1.29 ± 0.06	18.9 ± 0.9	7.57	12.7	87.3
	1 month	0.158 ± 0.005	1.389 ± 0.04	88.6 ± 0.5	226 ± 11	1.07 ± 0.05	16.9 ± 0.8	5.59	13.8	86.2
	3 months	0.150 ± 0.006	1.414 ± 0.05	89.4 ± 0.5	85 ± 4	0.43 ± 0.02	18.4 ± 0.9	5.94	4.9	95.1
Z2	*No storage*	0.120 ± 0.006	1.465 ± 0.01	91.8 ± 0.4	226 ± 11	1.25 ± 0.06	19.0 ± 1.0	7.62	11.0	89.0
	1 month	0.134 ± 0.009	1.394 ± 0.03	90.4 ± 0.7	164 ± 8	0.87 ± 0.04	18.0 ± 0.9	6.76	8.6	91.4
	3 months	0.135 ± 0.006	1.433 ± 0.04	90.6 ± 0.5	120 ± 6	0.60 ± 0.03	16.5 ± 0.8	6.69	6.4	93.6
Z3	*No storage*	0.172 ± 0.006	1.385 ± 0.02	87.6 ± 0.5	204 ± 10	1.18 ± 0.06	19.9 ± 1.0	5.08	16.0	84.0
	1 month	0.182 ± 0.006	1.369 ± 0.03	86.7 ± 0.5	184 ± 9	0.97 ± 0.05	17.3 ± 0.9	4.78	14.5	85.5
	3 months	0.176 ± 0.007	1.360 ± 0.01	87.0 ± 0.5	178 ± 9	0.98 ± 0.05	17.8 ± 0.9	4.93	15.1	84.9
Z4	*No storage*	0.192 ± 0.016	1.353 ± 0.02	85.8 ± 1.2	226 ± 11	1.35 ± 0.07	19.0 ± 0.9	4.46	22.5	77.5
	1 month	0.197 ± 0.002	1.350 ± 0.03	85.4 ± 0.4	207 ± 10	1.30 ± 0.07	21.2 ± 1.1	4.35	20.1	79.9
	3 months	0.187 ± 0.008	1.303 ± 0.03	85.6 ± 0.7	157 ± 8	0.91 ± 0.05	19.0 ± 0.9	4.58	15.1	84.9

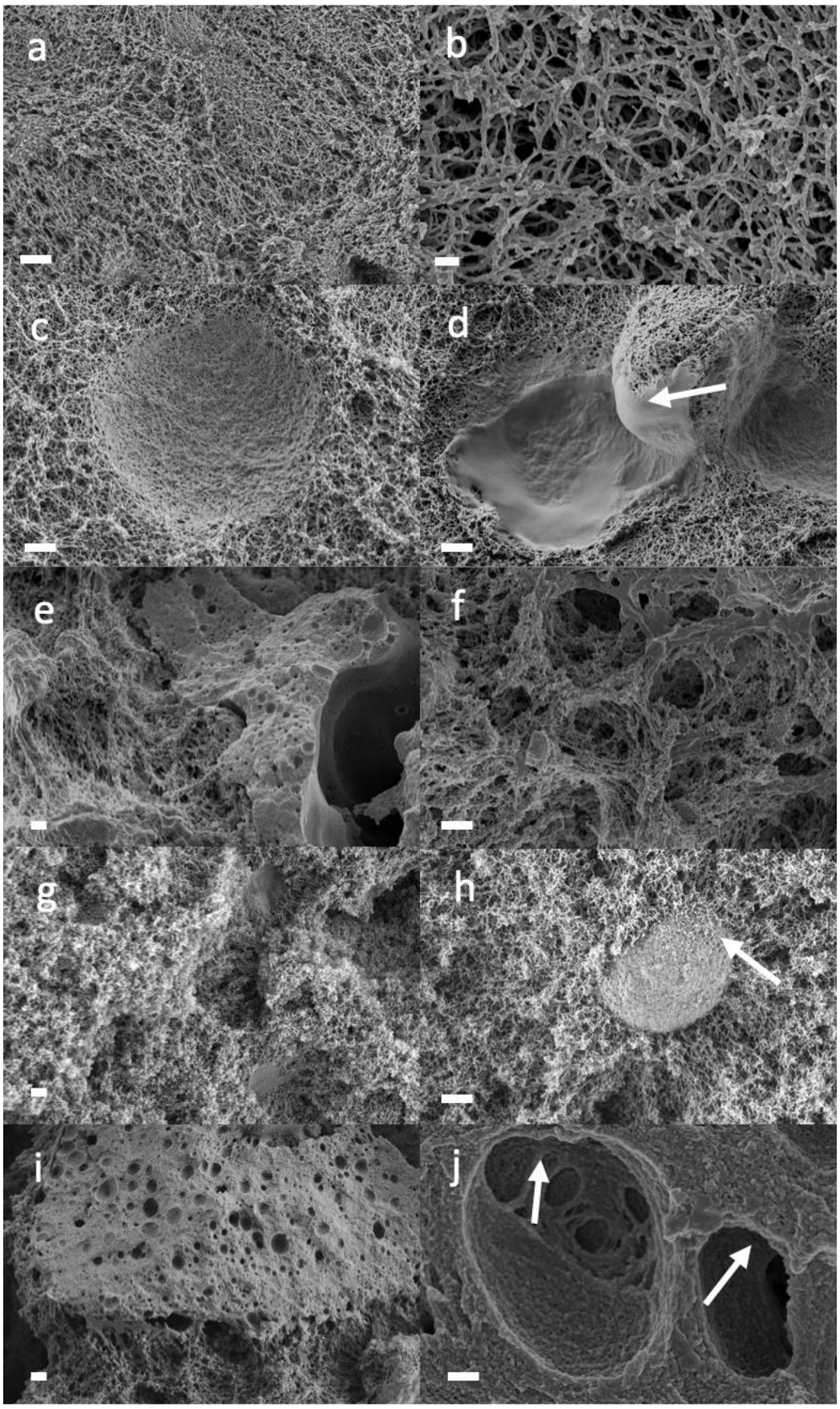

267

Figure 3. SEM images of horizontal cross-sections of the obtained starch-based aerogels. (a,b) Characteristic microstructure of unmodified aerogels (Z0). (c,d) The addition of low contents of the porogen (Z1) and later leaching induced the formation of larger pores with rough inner surfaces, although thin films of zein residues could be observed along the aerogel (d, arrow). (e,f) More residues were detected for Z2 in certain areas, but an interconnected porous network was obtained. (g,h) The incorporation of higher zein amounts (Z3) leads to more irregular surfaces and entire spherical zein particles were identified (h, arrow), highlighting the uncompleted porogen leaching. (i,j) Z4 aerogel formulation presented numerous porous zein plates well-integrated with the starch network backbone. (j) In addition, larger and interconnected pores (arrows) with noticeable roughness were obtained. Scale bars: 300 nm (b, j) and 2 μm (a, c-i).

Mechanical characterization of starch aerogels. All starch aerogel formulations were subjected to uniaxial quasistatic compressions of up to 70 % strain (Figure 4). The mechanical response of the aerogels showed an irregular nature subject to addition of the zein component. Considering the pure starch aerogel (Z0) as the reference, the curves corresponding to Z1 and Z2 showed that the addition of zein strongly softened their stress-strain response. This behavior is clearly related to the formation of hollow spaces in the starch aerogel backbone (Figure 3). However, this softening trend was reversed for the case of the aerogels with higher zein residues (Z3, Z4 in Table 2) and its stiffness was strongly enhanced. For instance, the stiffness of the starch aerogel processed with the highest zein content (Z4) was even stronger than the reference aerogel Z0. The compression moduli of the five aerogel formulations are illustrated in Figure 4 to quantitatively show this effect. A polynomial fit expressing the relation between Young's

modulus under compression (given in MPa) and the zein-to-starch ratio is expressed as follows (Eq. 4)

$$E(c) = -4.2157c^3 + 12.1715c^2 - 7.1856c + 2.0639 \quad (4)$$

where c varies from 0 to 1 and denotes the zein-to-starch weight ratio (Table 1). For the aerogels in consideration, an explanation to the trend seen in Figure 5 can be deduced from the bulk density measurements in Table 3. Porous materials, such as aerogels, exhibit a power-law scaling relation between Young's modulus E and the bulk density (ρ_{bulk}) [38–40]. Such scaling behavior is also specifically observed in other polysaccharide-based aerogels [41–45]. Table 3 shows the effect of zein on the bulk densities of the aerogels, where a decreasing trend from Z0→Z1→Z2 and an increasing trend from Z2→Z3→Z4 were observed. This explains the trend of Young's modulus *vs.* the zein-to-starch weight ratio (density) curve. The addition of zein as a porogen induced the formation of macropores, which also influenced the overall macroscopic mechanical behavior of the aerogels. Such influence of the hierarchical porous structure on the mechanical behavior was previously reported for cellulose aerogels [46].

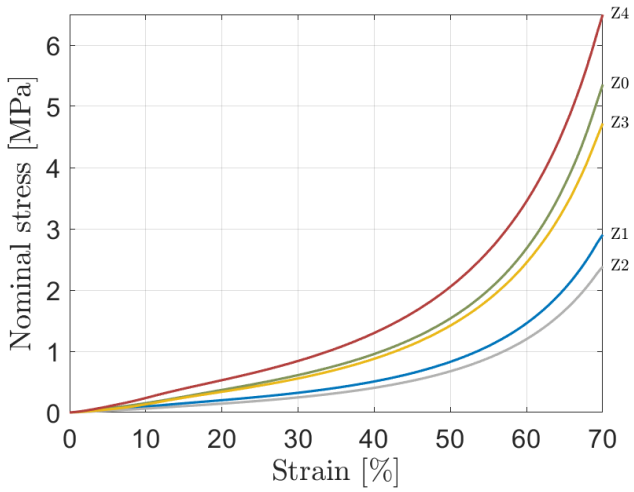

Figure 4. Stress-strain curves of starch aerogels processed with different zein contents (Z0 to Z4 with increasing zein content) tested under compression.

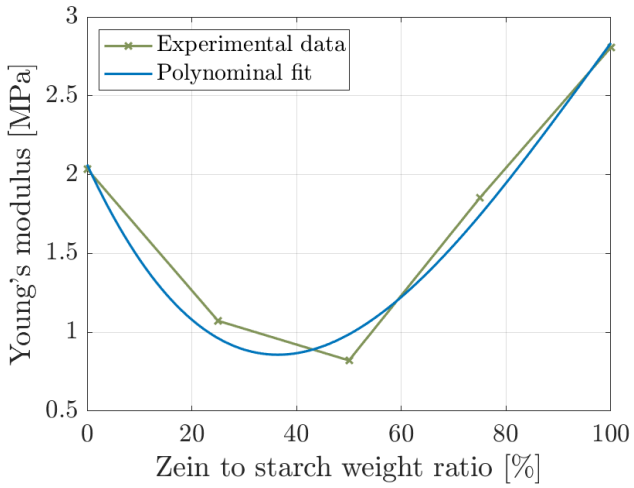

Figure 5. Effect of the zein content used during the starch aerogel processing on Young's moduli of the aerogels. A polynomial fit is generated to show the relation between the zein-to-starch weight ratio (in percentage, adhering to Eq. (4)) to Young's modulus.

Under cyclic loading, all the tested aerogels show typical elastoplastic behavior, with very large permanent set (Figures 6 and S4). This behavior is typical of other biopolymer-based aerogels [43]. The very small hysteresis (area between the unloading curve of a cycle and the reloading curve of the subsequent cycle) along with the permanent set indicate severe irreversible damage within the microstructure of the aerogel network. However, the aerogels exhibit a good strain memory as the reloading curve comes back to the point of the maximal strain of the previous loading cycle and continues the path as if it were the monotonic loading (Figure 6).

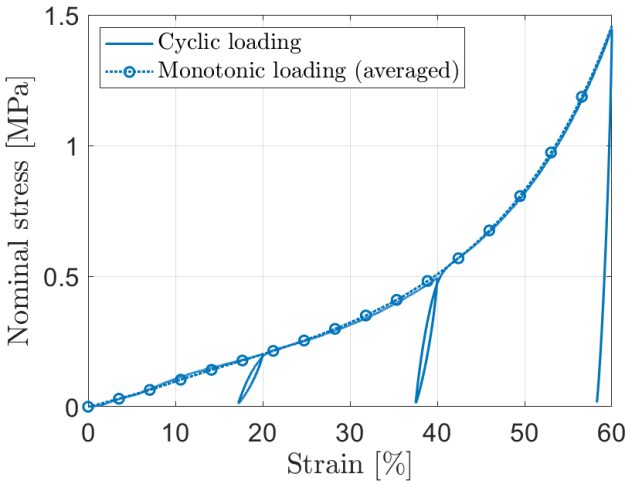

Figure 6. Stress-strain response of Z1 aerogels under cyclic loading-unloading quasistatic compression. The specimen was subjected to three sets of loading cycles with the strain amplitude increased stepwise by 20 %. The monotonic loading curve is illustrated as a dotted line, demonstrating a memory of the aerogels. Curves of the other tested formulations (Z0, Z2, Z3 and Z4) showed a similar behavior and can be found as supplementary material (Figure S4).

Effect of storage time. The stability under storage of drug products, medical devices and combination products (i.e. products comprising a drug and a medical device, or a biological product and a medical device) is a critical quality parameter within a well-established legal framework, since the variety of degradation processes (chemical, physical, biopharmaceutical) that may occur could render products ineffective or unsafe before patient use [22]. Nevertheless, there is paucity of information on research regarding the stability of complex porous architectures conceived as scaffolds [47].

The exposition to the storage conditions induced certain volume shrinkage of the starch aerogels. Formulations containing higher zein residues (Z3, Z4) presented values identical to their non-stored counterparts, thus preserving their initial structure. On the other hand, higher

volume shrinkages close to 5 % were observed for unmodified aerogels (Z0) after 3 months of storage (Figure 7).

After 1 month of storage at 25 ºC and 65 % relative humidity, aerogels experienced a densification in the 3-32 % range, depending on the formulation (Table 3). The highest densification was reached for Z1 aerogel, whereas this effect was very low in formulations with higher initial zein-to-starch weight ratio (Z2-Z4). This preventive effect can be directly attributed to the zein residues (Table 2).

Interestingly, bulk densities of aerogels after 3 months were lower than after 1 month, regardless the aerogel composition. The incorporation of higher amounts of zein reduced the storage impact, obtaining slightly lighter structures for Z4 after 3 months of storage. Overall, all manufactured aerogels experienced a densification and a mild reduction in the overall porosity after the storage period (Table 3).

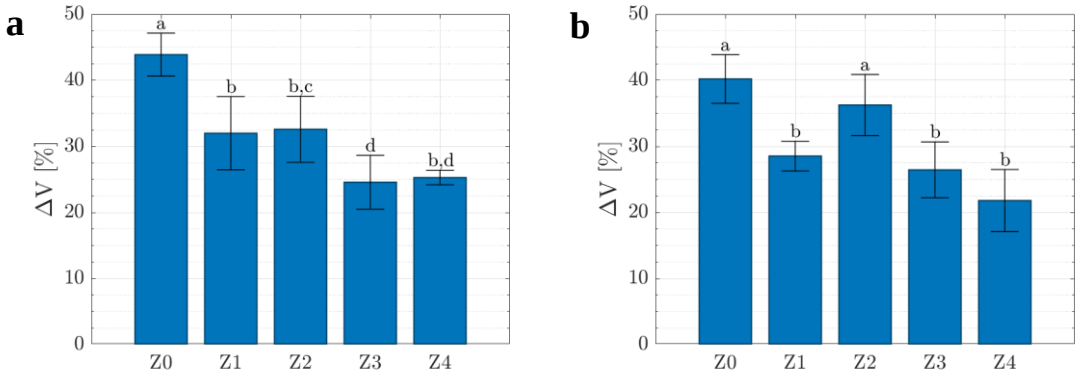

Figure 7. Overall shrinkage values of starch aerogels after the storage periods of (a) 1 month and (b) 3 months. Equal letters denote statistically homogeneous groups.

The densification of the aerogels after the storage had a parallel impact on the textural properties, with consistent decreases in the specific surface areas (A_{BET} in Table 3). Aerogel formulations containing zein presented a reduction in the $V_{p,BJH}$ values. This is attributed to the

swelling ability of amylopectin in humid environment that would cause the pore collapse, mainly affecting the smaller pore population [48]. In general, the impact of storage on the aerogel formulations depended on the remaining porogen traces. In Z1 and Z2, the major part of the zein was leached during the aerogel processing, leading to a more open structure and thus favoring the water intake, as suggested by both the remarkable decrease in $V_{p,\ BJH}$ and the increase in the $V_{p,macro}$ values. The presence of hydrophobic zein residues along the aerogel monoliths may hinder the starch interaction with the moisture [49]. Accordingly, Z3 and Z4 aerogels had less drastic variations in the textural properties. For instance, $V_{p,macro}$ of Z3 aerogels after 3 months of storage was nearly identical to its non-stored counterpart.

After the storage period (1 and 3 months), aerogels were tested again under quasistatic compression. Despite the abovementioned morphological changes mainly in the smaller pore population (micropores), their mechanical performance was virtually unaffected after the storage period under 25 °C and 65 % relative humidity (Figure 8). In previous theoretical studies on modeling of biopolymer aerogels [40,50], it was proposed that pores (cellular fiber-network) within the microporous region and lower mesoporous region do not play a significant role in the overall mechanical performance of the aerogels. This could explain the absence of an effect on the stress-strain response due to a reduction in the amount of micropores and lower mesopores. The result illustrated in Figure 8 opens up questions that need further investigations by theoretical and experimental approaches. The stored aerogels were further subjected to cyclic loading and showed similar elastoplastic behavior as that of the non-stored aerogels.

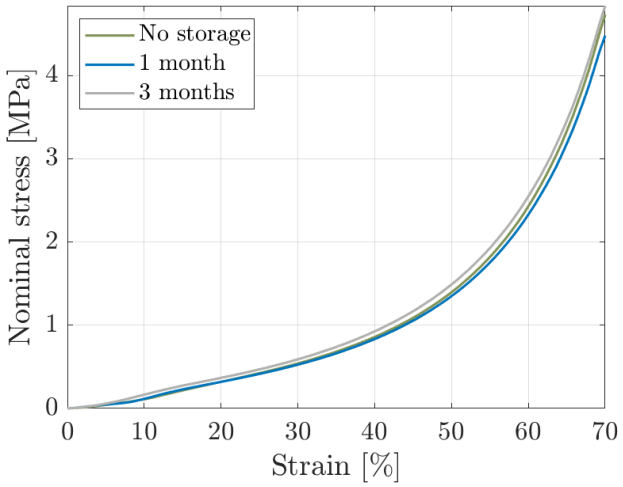

Figure 8. Uniaxial quasistatic compression curves of starch aerogel (Z3) specimens subject to different storage duration (0, 1 and 3 months) at 25 ºC and 65 % relative humidity. Curves for the rest of aerogels can be found in the supplementary information (Figure S5).

CONCLUSIONS

Starch aerogels displaying a new macropore population (1-2 µm) were successfully manufactured by the incorporation of zein as a porogen. Highly porous aerogels (85-92 %) were obtained with well-integrated macropores in the mesoporous starch aerogel backbone, encouraging its use as scaffolds for tissue engineering applications. Zein incorporation induced remarkable changes in the mechanical performance of the end aerogel products with an enhanced stiffness. The storage period mimicking the ICH-climatic conditions of Europe, USA and Japan induced morphological modifications in the aerogels whilst the mechanical behavior was virtually unaffected. The presence of zein residues along the aerogel scaffolds had a preventive effect on the morphological changes during the storage period. Overall, zein appears as an advantageous biocompatible porogen for the processing of dual-porous starch aerogels from the

technological (integration in classical aerogel processing pathway without extra-leaching steps) and materials performance (enhanced stiffness and stability) points of view.

ASSOCIATED CONTENT

Supporting Information. Pore size distributions from BJH-desorption, physical appearance of aerogel, HPLC-QTOF-MS/MS fragmentation spectra of target peptides, compressive behavior of starch aerogel composites under cyclic loading and different storage time periods.

AUTHOR INFORMATION

Corresponding Authors

* Carlos A. García-González. *carlos.garcia@usc.es, *Tel.: +34-881-814882*

** Ameya Rege. **ameya.rege@dlr.de, *Tel.: +49-2203-6015158*

Author Contributions

The manuscript was written through contributions of all authors. All authors have given approval to the final version of the manuscript.

Notes

The authors declare no competing financial interest.

ACKNOWLEDGEMENTS

This research was funded by Xunta de Galicia [ED431F 2016/010; ED431C 2020/17], MCIUN [RTI2018-094131-A-I00], Agrupación Estratégica de Materiales [AeMAT-BIOMEDCO2, ED431E 2018/08], Agencia Estatal de Investigación [AEI] and FEDER funds. V. Santos-Rosales acknowledges to Xunta de Galicia (Consellería de Cultura, Educación e Ordenación Universitaria) for a predoctoral research fellowship [ED481A-2018/014]. C.A. García-González acknowledges to MINECO for a Ramón y Cajal Fellowship [RYC2014-15239]. Authors would like to thank Roquette (Spain) for kindly providing the starch and to Plataforma Proteómica-Metabolómica (CEI-UAM+CSIC) for the zein analysis. Work carried out in the frame of the COST Action CA18125 "Advanced Engineering and Research of aeroGels for Environment and Life Sciences" (AERoGELS) and funded by the European Commission.

REFERENCES

(1) Jafari, M.; Paknejad, Z.; Rad, M. R.; Motamedian, S. R.; Eghbal, M. J.; Nadjmi, N.; Khojasteh, A. Polymeric Scaffolds in Tissue Engineering: A Literature Review: Polymeric Scaffolds in Tissue Engineering. *Journal of Biomedical Materials Research Part B: Applied Biomaterials* **2017**, *105* (2), 431–459. https://doi.org/10.1002/jbm.b.33547.

(2) Loh, Q. L.; Choong, C. Three-Dimensional Scaffolds for Tissue Engineering Applications: Role of Porosity and Pore Size. *Tissue Engineering Part B: Reviews* **2013**, *19* (6), 485–502. https://doi.org/10.1089/ten.teb.2012.0437.

(3) Santos-Rosales, V.; Iglesias-Mejuto, A.; García-González, C. A. Solvent-Free Approaches for the Processing of Scaffolds in Regenerative Medicine. *Polymers* **2020**, *12* (3), 533. https://doi.org/10.3390/polym12030533.

(4) García-González, C. A.; Concheiro, A.; Alvarez-Lorenzo, C. Processing of Materials for Regenerative Medicine Using Supercritical Fluid Technology. *Bioconjugate Chem.* **2015**, *26* (7), 1159–1171. https://doi.org/10.1021/bc5005922.

(5) Maleki, H.; Durães, L.; García-González, C. A.; del Gaudio, P.; Portugal, A.; Mahmoudi, M. Synthesis and Biomedical Applications of Aerogels: Possibilities and Challenges. *Advances in Colloid and Interface Science* **2016**, *236*, 1–27. https://doi.org/10.1016/j.cis.2016.05.011.

(6) Ganesan, K.; Budtova, T.; Ratke, L.; Gurikov, P.; Baudron, V.; Preibisch, I.; Niemeyer, P.; Smirnova, I.; Milow, B. Review on the Production of Polysaccharide Aerogel Particles. *Materials* **2018**, *11* (11), 2144. https://doi.org/10.3390/ma11112144.

(7) Randall, J. P.; Meador, M. A. B.; Jana, S. C. Tailoring Mechanical Properties of Aerogels for Aerospace Applications. *ACS Applied Materials & Interfaces* **2011**, *3* (3), 613–626. https://doi.org/10.1021/am200007n.

(8) Koebel, M.; Rigacci, A.; Achard, P. Aerogel-Based Thermal Superinsulation: An Overview. *Journal of Sol-Gel Science and Technology* **2012**, *63* (3), 315–339. https://doi.org/10.1007/s10971-012-2792-9.

(9) García-González, C. A.; Budtova, T.; Durães, L.; Erkey, C.; Del Gaudio, P.; Gurikov, P.; Koebel, M.; Liebner, F.; Neagu, M.; Smirnova, I. An Opinion Paper on Aerogels for Biomedical and Environmental Applications. *Molecules* **2019**, *24* (9), 1815. https://doi.org/10.3390/molecules24091815.

(10) Zhu, F. Starch Based Aerogels: Production, Properties and Applications. *Trends in Food Science & Technology* **2019**, *89*, 1–10. https://doi.org/10.1016/j.tifs.2019.05.001.

(11) García-González, C. A.; Alnaief, M.; Smirnova, I. Polysaccharide-Based Aerogels—Promising Biodegradable Carriers for Drug Delivery Systems. *Carbohydrate Polymers* **2011**, *86* (4), 1425–1438. https://doi.org/10.1016/j.carbpol.2011.06.066.

(12) Mehling, T.; Smirnova, I.; Guenther, U.; Neubert, R. H. H. Polysaccharide-Based Aerogels as Drug Carriers. *Journal of Non-Crystalline Solids* **2009**, *355* (50–51), 2472–2479. https://doi.org/10.1016/j.jnoncrysol.2009.08.038.

(13) García-González, C. A.; López-Iglesias, C.; Concheiro, A.; Alvarez-Lorenzo, C. Chapter 16. Biomedical Applications of Polysaccharide and Protein Based Aerogels. In *Green Chemistry Series*; Thomas, S., Pothan, L. A., Mavelil-Sam, R., Eds.; Royal Society of Chemistry: Cambridge, 2018; pp 295–323. https://doi.org/10.1039/9781782629979-00295.

(14) Silva, G. A.; Coutinho, O. P.; Ducheyne, P.; Shapiro, I. M.; Reis, R. L. The Effect of Starch and Starch-Bioactive Glass Composite Microparticles on the Adhesion and Expression of the Osteoblastic Phenotype of a Bone Cell Line. *Biomaterials* **2007**, *28* (2), 326–334. https://doi.org/10.1016/j.biomaterials.2006.07.009.

(15) Zhang, R.; Ma, P. X. Synthetic Nano-Fibrillar Extracellular Matrices with Predesigned Macroporous Architectures. *J. Biomed. Mater. Res.* **2000**, *52* (2), 430–438.

(16) Reverchon, E.; Cardea, S.; Rapuano, C. A New Supercritical Fluid-Based Process to Produce Scaffolds for Tissue Replacement. *The Journal of Supercritical Fluids* **2008**, *45* (3), 365–373. https://doi.org/10.1016/j.supflu.2008.01.005.

(17) Baldino, L.; Naddeo, F.; Cardea, S.; Naddeo, A.; Reverchon, E. FEM Modeling of the Reinforcement Mechanism of Hydroxyapatite in PLLA Scaffolds Produced by Supercritical

Drying, for Tissue Engineering Applications. *Journal of the Mechanical Behavior of Biomedical Materials* **2015**, *51*, 225–236. https://doi.org/10.1016/j.jmbbm.2015.07.021.

(18) Ma, Z.; Gao, C.; Gong, Y.; Shen, J. Paraffin Spheres as Porogen to Fabricate Poly(L-Lactic Acid) Scaffolds with Improved Cytocompatibility for Cartilage Tissue Engineering. *Journal of Biomedical Materials Research* **2003**, *67B* (1), 610–617. https://doi.org/10.1002/jbm.b.10049.

(19) *Modern Pharmaceutics*, 4th ed., rev.expanded.; Banker, G. S., Rhodes, C. T., Eds.; Drugs and the pharmaceutical sciences; Marcel Dekker: New York, 2002.

(20) Wang, H.; Gong, S.; Lin, Z.; Fu, J.; Xue, S.; Huang, J.; Wang, J. In Vivo Biocompatibility and Mechanical Properties of Porous Zein Scaffolds. *Biomaterials* **2007**, *28* (27), 3952–3964. https://doi.org/10.1016/j.biomaterials.2007.05.017.

(21) Tu, J.; Wang, H.; Li, H.; Dai, K.; Wang, J.; Zhang, X. The in Vivo Bone Formation by Mesenchymal Stem Cells in Zein Scaffolds. *Biomaterials* **2009**, *30* (26), 4369–4376. https://doi.org/10.1016/j.biomaterials.2009.04.054.

(22) Kommanaboyina, B.; Rhodes, C. T. Trends in Stability Testing, with Emphasis on Stability During Distribution and Storage. *Drug Development and Industrial Pharmacy* **1999**, *25* (7), 857–868. https://doi.org/10.1081/DDC-100102246.

(23) Santos-Rosales, V.; Ardao, I.; Alvarez-Lorenzo, C.; Ribeiro, N.; Oliveira, A.; García-González, C. Sterile and Dual-Porous Aerogels Scaffolds Obtained through a Multistep Supercritical CO2-Based Approach. *Molecules* **2019**, *24* (5), 871. https://doi.org/10.3390/molecules24050871.

(24) Wilson, R. E. Humidity Control by Means of Sulfuric Acid Solutions, with Critical Compilation of Vapor Pressure Data. *Journal of Industrial & Engineering Chemistry* **1921**, *13* (4), 326–331. https://doi.org/10.1021/ie50136a022.

(25) Wang, S.; Li, C.; Copeland, L.; Niu, Q.; Wang, S. Starch Retrogradation: A Comprehensive Review: Starch Retrogradation…. *Comprehensive Reviews in Food Science and Food Safety* **2015**, *14* (5), 568–585. https://doi.org/10.1111/1541-4337.12143.

(26) García-González, C. A.; Smirnova, I. Use of Supercritical Fluid Technology for the Production of Tailor-Made Aerogel Particles for Delivery Systems. *The Journal of Supercritical Fluids* **2013**, *79*, 152–158. https://doi.org/10.1016/j.supflu.2013.03.001.

(27) Druel, L.; Bardl, R.; Vorwerg, W.; Budtova, T. Starch Aerogels: A Member of the Family of Thermal Superinsulating Materials. *Biomacromolecules* **2017**, *18* (12), 4232–4239. https://doi.org/10.1021/acs.biomac.7b01272.

(28) Ma, P. X. Scaffolds for Tissue Fabrication. *Materials Today* **2004**, *7* (5), 30–40. https://doi.org/10.1016/S1369-7021(04)00233-0.

(29) García-González, C. A.; Uy, J. J.; Alnaief, M.; Smirnova, I. Preparation of Tailor-Made Starch-Based Aerogel Microspheres by the Emulsion-Gelation Method. *Carbohydrate Polymers* **2012**, *88* (4), 1378–1386. https://doi.org/10.1016/j.carbpol.2012.02.023.

(30) Rudaz, C.; Courson, R.; Bonnet, L.; Calas-Etienne, S.; Sallée, H.; Budtova, T. Aeropectin: Fully Biomass-Based Mechanically Strong and Thermal Superinsulating Aerogel. *Biomacromolecules* **2014**, *15* (6), 2188–2195. https://doi.org/10.1021/bm500345u.

(31) Budtova, T. Cellulose II Aerogels: A Review. *Cellulose* **2019**, *26* (1), 81–121. https://doi.org/10.1007/s10570-018-2189-1.

(32) Miao, Z.; Ding, K.; Wu, T.; Liu, Z.; Han, B.; An, G.; Miao, S.; Yang, G. Fabrication of 3D-Networks of Native Starch and Their Application to Produce Porous Inorganic Oxide Networks through a Supercritical Route. *Microporous and Mesoporous Materials* **2008**, *111* (1–3), 104–109. https://doi.org/10.1016/j.micromeso.2007.07.018.

(33) Cabra, V.; Arreguin, R.; Vazquez-Duhalt, R.; Farres, A. Effect of Temperature and PH on the Secondary Structure and Processes of Oligomerization of 19 KDa Alpha-Zein. *Biochimica et Biophysica Acta (BBA) - Proteins and Proteomics* **2006**, *1764* (6), 1110–1118. https://doi.org/10.1016/j.bbapap.2006.04.002.

(34) Sun, C.; Dai, L.; Liu, F.; Gao, Y. Simultaneous Treatment of Heat and High Pressure Homogenization of Zein in Ethanol–Water Solution: Physical, Structural, Thermal and Morphological Characteristics. *Innovative Food Science & Emerging Technologies* **2016**, *34*, 161–170. https://doi.org/10.1016/j.ifset.2016.01.016.

(35) Zhang, J.; Wen, C.; Zhang, H.; Zandile, M.; Luo, X.; Duan, Y.; Ma, H. Structure of the Zein Protein as Treated with Subcritical Water. *International Journal of Food Properties* **2018**, *21* (1), 128–138. https://doi.org/10.1080/10942912.2017.1414839.

(36) Shukla, R.; Cheryan, M. Zein: The Industrial Protein from Corn. *Industrial Crops and Products* **2001**, *13* (3), 171–192. https://doi.org/10.1016/S0926-6690(00)00064-9.

(37) Pascoli, M.; de Lima, R.; Fraceto, L. F. Zein Nanoparticles and Strategies to Improve Colloidal Stability: A Mini-Review. *Frontiers in Chemistry* **2018**, *6*. https://doi.org/10.3389/fchem.2018.00006.

(38) Gibson, L. J.; Ashby, M. F. *Cellular Solids: Structure and Properties*, 2nd ed.; Cambridge University Press, 1997. https://doi.org/10.1017/CBO9781139878326.

(39) Groβ, J.; Fricke, J. Scaling of Elastic Properties in Highly Porous Nanostructured Aerogels. *Nanostructured Materials* **1995**, *6* (5–8), 905–908. https://doi.org/10.1016/0965-9773(95)00206-5.

(40) Rege, A.; Schestakow, M.; Karadagli, I.; Ratke, L.; Itskov, M. Micro-Mechanical Modelling of Cellulose Aerogels from Molten Salt Hydrates. *Soft Matter* **2016**, *12* (34), 7079–7088. https://doi.org/10.1039/C6SM01460G.

(41) Karadagli, I.; Schulz, B.; Schestakow, M.; Milow, B.; Gries, T.; Ratke, L. Production of Porous Cellulose Aerogel Fibers by an Extrusion Process. *The Journal of Supercritical Fluids* **2015**, *106*, 105–114. https://doi.org/10.1016/j.supflu.2015.06.011.

(42) Plappert, S. F.; Nedelec, J.-M.; Rennhofer, H.; Lichtenegger, H. C.; Liebner, F. W. Strain Hardening and Pore Size Harmonization by Uniaxial Densification: A Facile Approach toward Superinsulating Aerogels from Nematic Nanofibrillated 2,3-Dicarboxyl Cellulose. *Chemistry of Materials* **2017**, *29* (16), 6630–6641. https://doi.org/10.1021/acs.chemmater.7b00787.

(43) Zhao, S.; Malfait, W. J.; Guerrero-Alburquerque, N.; Koebel, M. M.; Nyström, G. Biopolymer Aerogels and Foams: Chemistry, Properties, and Applications. *Angewandte Chemie International Edition* **2018**, *57* (26), 7580–7608. https://doi.org/10.1002/anie.201709014.

(44) Rege, A.; Ratke, L.; Itskov, M. Chapter 8. Modelling and Simulations of Polysaccharide and Protein Based Aerogels. In *Green Chemistry Series*; Thomas, S., Pothan, L. A., Mavelil-Sam, R., Eds.; Royal Society of Chemistry: Cambridge, 2018; pp 129–150. https://doi.org/10.1039/9781782629979-00129.

(45) Buchtová, N.; Pradille, C.; Bouvard, J.-L.; Budtova, T. Mechanical Properties of Cellulose Aerogels and Cryogels. *Soft Matter* **2019**, *15* (39), 7901–7908. https://doi.org/10.1039/C9SM01028A.

(46) Ganesan, K.; Barowski, A.; Ratke, L.; Milow, B. Influence of Hierarchical Porous Structures on the Mechanical Properties of Cellulose Aerogels. *Journal of Sol-Gel Science and Technology* **2019**, *89* (1), 156–165. https://doi.org/10.1007/s10971-018-4828-2.

(47) Goimil, L.; Jaeger, P.; Ardao, I.; Gómez-Amoza, J. L.; Concheiro, A.; Alvarez-Lorenzo, C.; García-González, C. A. Preparation and Stability of Dexamethasone-Loaded Polymeric Scaffolds for Bone Regeneration Processed by Compressed CO2 Foaming. *Journal of CO2 Utilization* **2018**, *24*, 89–98. https://doi.org/10.1016/j.jcou.2017.12.012.

(48) Alcázar-Alay, S. C.; Meireles, M. A. A. Physicochemical Properties, Modifications and Applications of Starches from Different Botanical Sources. *Food Science and Technology (Campinas)* **2015**, *35* (2), 215–236. https://doi.org/10.1590/1678-457X.6749.

(49) Savich, I. M. Hydrophobic Properties of Maize Zein. *Chemistry of Natural Compounds* **1991**, *27* (1), 92–95. https://doi.org/10.1007/BF00629841.

(50) Rege, A.; Hillgärtner, M.; Itskov, M. Mechanics of Biopolymer Aerogels Based on Microstructures Generated from 2-d Voronoi Tessellations. *The Journal of Supercritical Fluids* **2019**, *151*, 24–29. https://doi.org/10.1016/j.supflu.2019.04.018.